

The S2N2 metallicity calibrator and the abundance gradient of M 33

K. Viironen^{1*}, G. Delgado-Inglada², A. Mampaso¹,
L. Magrini³ and R. L. M. Corradi^{4,1}

¹*Instituto de Astrofísica de Canarias (IAC), C/ Vía Láctea s/n, 38200 La Laguna, Tenerife, Spain*

²*Instituto Nacional de Astrofísica, Óptica y Electrónica (INAOE), Luis Enrique Erro 1, Tonantzintla, Puebla, Mexico*

³*INAF-Osservatorio Astrofisico di Arcetri, Largo E. Fermi, 5 50125, Firenze, Italy*

⁴*Isaac Newton Group of Telescopes, Apartado de Correos 321, E-38700 Sta. Cruz de La Palma, Spain*

Accepted ?. Received ?; in original form ?

ABSTRACT

We introduce the $\log(\text{H}\alpha/[\text{S II}]\lambda\lambda 6717+6731)$ vs. $\log(\text{H}\alpha/[\text{N II}]\lambda 6583)$ (S2N2) diagnostic diagram as metallicity and ionisation parameter indicator for H II regions in external galaxies. The location of H II regions in the S2N2 diagram was studied both empirically and theoretically. We found that, for a wide range of metallicities, the S2N2 diagram gives single valued results in the metallicity-ionisation parameter plane. We demonstrate that the S2N2 diagram is a powerful tool to estimate metallicities of high-redshift ($z \sim 2$) H II galaxies. Finally, we derive the metallicity for 76 H II regions in M33 from the S2N2 diagram and calculate an O/H abundance gradient for this galaxy of $-0.05 (\pm 0.01)$ dex kpc⁻¹.

Key words: H II regions – galaxies: abundances – galaxies: individual: M33 – galaxies: high-redshift

1 INTRODUCTION

Chemical abundances of the ionised interstellar medium in our own and in external galaxies are commonly studied by analysing the emission line spectra of their H II regions. This task is relatively straightforward if the lines for the electron temperature determination can be measured directly from the observations. However, these auroral lines (like $[\text{N II}]\lambda 5755$ or $[\text{O III}]\lambda 4363$) are usually too faint to be detected for distant H II regions, and especially in high metallicity regions. This has woken an interest in having abundance indicators based on strong lines only. The use of these strong-line methods was pioneered by Pagel et al. (1979) and Alloin et al. (1979), followed later by numerous studies from different authors. The lines most commonly used are oxygen ($[\text{O II}]\lambda\lambda 3727, 3729$, $[\text{O III}]\lambda\lambda 4959, 5007$), nitrogen ($[\text{N II}]\lambda 6583$), and sulphur ($[\text{S II}]\lambda\lambda 6717, 6731$, $[\text{S III}]\lambda\lambda 6312, 9069, 9532$), normalised to the hydrogen lines ($\text{H}\alpha\lambda 6563$, $\text{H}\beta\lambda 4861$) (Kewley & Dopita 2002). Recently, Stasińska (2006) presented two new oxygen abundance indicators based on argon and sulphur lines: $[\text{Ar III}]/[\text{O III}]$ and $[\text{S III}]/[\text{O III}]$.

In this paper we study the $\log(\text{H}\alpha/[\text{S II}]\lambda\lambda 6717+6731)$

vs. $\log(\text{H}\alpha/[\text{N II}]\lambda 6583)$ diagram (referred to as S2N2 in the following) as a metallicity indicator. This diagram was introduced by Sabbadin et al. (1977) as a useful tool to separate galactic planetary nebulae (PNe), H II regions, and SNRs from each others, and was later applied to Herbig-Haro objects by Cantó (1981), to galactic PNe by García-Lario et al. (1991) and Riesgo & López (2005), and to extragalactic PNe by Magrini et al. (2003). Raimann et al. (2000) found a correlation between $[\text{N II}]/\text{H}\alpha$ and the metallicity for a sample of H II galaxies. A similar correlation was found by van Zee (2000) for a sample of dwarf galaxies and extra-galactic H II regions, and was further studied by several authors (e.g. Denicoló et al. 2002; Kewley & Dopita 2002; Melbourne & Salzer 2002; Pettini & Pagel 2004; Maier et al. 2005; Nagao et al. 2006). Diagrams combining $[\text{N II}]/\text{H}\alpha$ with $[\text{O III}]\lambda 5007/\text{H}\beta$ have been used in object classification by e.g. Contini et al. (2002); Maier et al. (2005); Groves et al. (2006), and Stasińska (2006). The $[\text{N II}]/\text{H}\alpha$ ratio has been used to determine ionisation parameter and metallicity in combination with several line ratios: $[\text{O III}]\lambda 5007/\text{H}\beta$ (e.g. Dopita et al. 2000; Kewley et al. 2001), $([\text{O II}]\lambda 3727 + [\text{O III}]\lambda\lambda 4959, 5007)/\text{H}\beta$ (R_{23}) (Melbourne & Salzer 2002; Lilly et al. 2003), and $[\text{O III}]\lambda\lambda 4959, 5007/[\text{O II}]\lambda 3727$ (O_{23}) (e.g. Lilly et al. 2003). On the other hand, Denicoló et al. (2002) demonstrated that the $[\text{S II}]/\text{H}\alpha$ line ratio is also correlated with the metallicity in a sample of H II re-

* E-mail: kerttu@iac.es (KV); gloria@inaoep.mx (GDI); amr@iac.es (AM); laura@arcetri.astro.it (LM); rcorradi@ing.iac.es (RLMC)

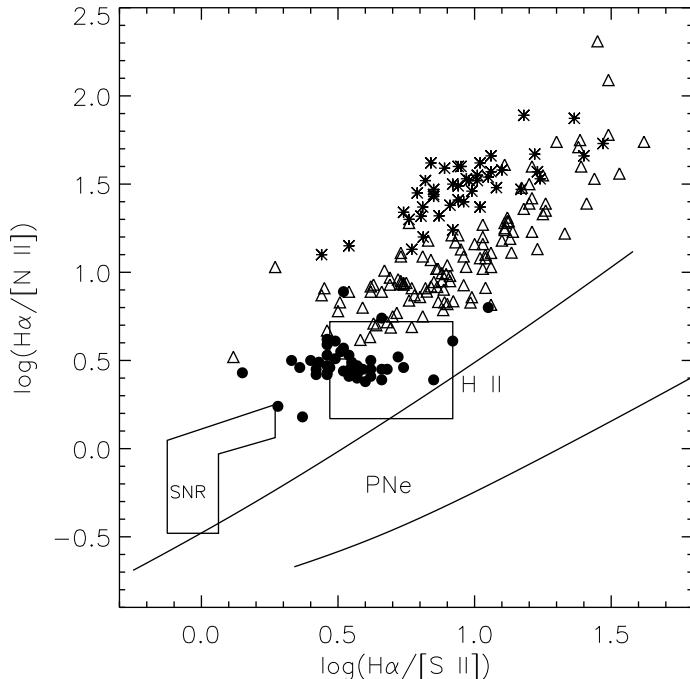


Figure 1. The loci of Galactic H II regions, SNRs and PNe (Sabbadin et al. 1977) in the S2N2 diagram. The Galactic H II regions occupy a very limited area in this diagram (the box labelled H II). Over-plotted is our sample of 205 extragalactic H II regions in Local Group galaxies coded according to the metallicity of their parent galaxies, in the following way: $7.30 \leq 12 + \log(\text{O}/\text{H}) \leq 8.06$ (stars), $8.06 < 12 + \log(\text{O}/\text{H}) \leq 8.40$ (triangles), $12 + \log(\text{O}/\text{H}) > 8.40$ (filled circles).

gions and galaxies. The use of a diagram combining $[\text{S II}]\lambda\lambda 6716, 6731/\text{H}\alpha$ with $[\text{O III}]/\text{H}\beta$ in object classification has been examined by e.g. Contini et al. (2002) and Stasińska (2006). The use of the same diagram for abundance and ionisation parameter diagnoses was studied e.g. by Dopita et al. (2000), and Kewley et al. (2001). Pérez-Montero & Díaz (2005) provide an analysis of the ranges of validity and average uncertainties for several line ratios used in nebular metallicity studies.

Delgado et al. (2005) first introduced the use of the S2N2 diagram for metallicity and ionisation parameter diagnoses for extragalactic H II regions. Moustakas & Kennicutt (2006) studied whether there was a difference between integrated spectra of galaxies and the spectra of individual H II regions when plotted in this diagram. Recently, Dopita et al. (2006) used the S2N2 diagram, among many others, for abundance diagnostics. They calculated time-dependent photo-ionisation models of individual H II regions and compared the models with H II region data from different authors.

In this paper we further explore the use of the S2N2 diagram for abundance and ionisation parameter diagnoses. We show that the diagram gives single valued results for a wide range of metallicities. A comparison of empirical H II region data with photo-ionisation (CLOUDY) model abundances is made, and a good fit between data and the models is found up to the highest abundances expected for H II regions. We also demonstrate that the S2N2 diagram is powerful enough to determine metallicities for high-redshift ($z \sim 2$) galaxies using current near-infrared spectrographs, and sensitive enough to measure with reasonable accuracy the O/H radial abundance gradient in M33.

2 OBSERVATIONAL DATA

2.1 Sample selection and properties

We have collected data for all H II regions in the Local Group galaxies for which adequate information about the emission lines needed was available. Data showing errors in the logarithmic line ratio ($\log(\text{H}\alpha/[\text{N II}])$ or $\log(\text{H}\alpha/[\text{S II}])$) greater than 0.15 dex were discarded. In the case of H II regions with various measurements from different authors, the most accurate measurements were adopted. Data for the galaxies Sextans A, Sextans B and NGC3109 were also included, although these galaxies are probably members of a small association of dwarf galaxies located just at the outskirts of the Local Group (Magrini 2006). In addition, the sample includes new data for 64 H II regions in M33 published recently by Magrini et al. (2007). Our final sample consists of 13 galaxies with a total of 205 well-measured H II regions. The sample galaxies, their magnitudes, O/H abundances and distances are presented in order of decreasing O/H abundance in Table 1. The data for the galaxies are adopted from van den Bergh (2000) except for Gr8 for which the magnitude and O/H abundance measurements are from van Zee et al. (2006), for EGB0427+63 (Hodge & Miller 1995) and for NGC 3109 (Richer & McCall 1995). The distance measurement for M33 is from Freedman et al. (1991). Data for individual H II regions and the corresponding references are given in Table A1.

Our sample is, in summary, limited to Local Group galaxies, i.e. to relatively nearby objects, so avoiding biases towards the brightest H II regions or to H II galaxies. Only spatially resolved H II regions are included, and the contribution from stars, clusters, and the diffuse ionised gas

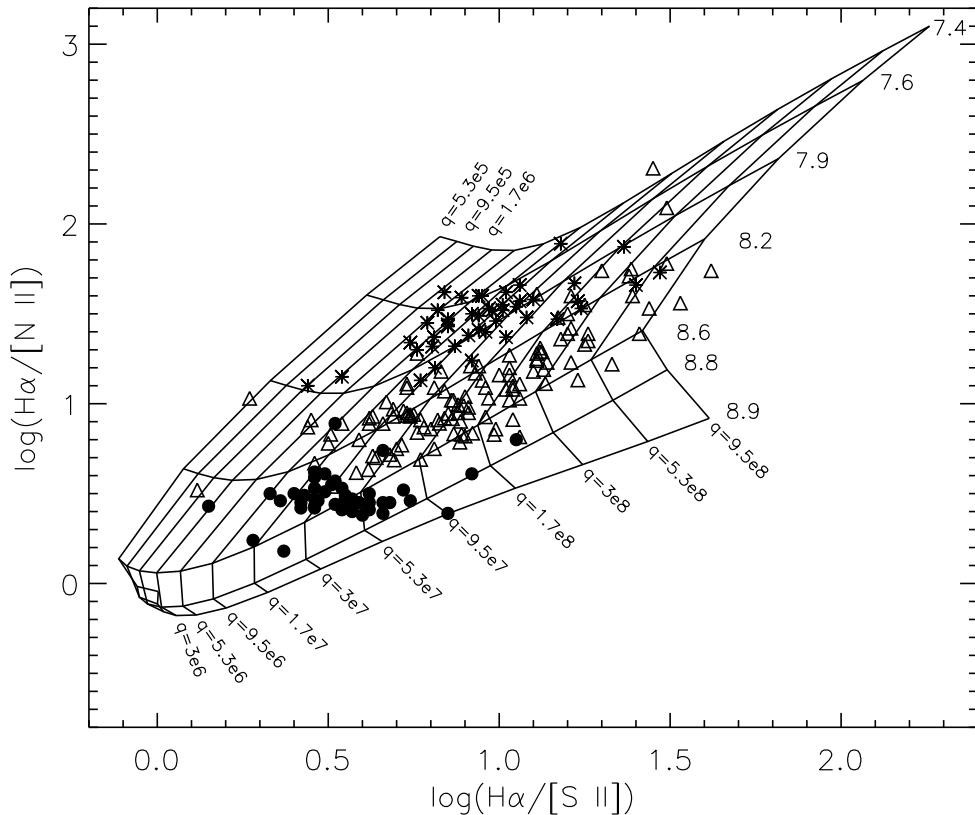


Figure 2. The H II region sample as in Fig. 1, over-plotted by the grid of photo-ionisation models. Labels indicate the values for the ionisation parameter ($5.3 \times 10^5 < q < 9.5 \times 10^8$) and oxygen abundance ($7.4 < 12 + \log(\text{O}/\text{H}) < 8.9$) used.

along the line of sight is minimised in the spectra. The sizes of the H II regions vary from compact to giant ones, and the sample coverage in luminosity and metallicity is broad: the galaxy magnitudes range from $M_V = -21.2$ (M31) to $M_V = -10.7$ (SagDIG), and the metallicities vary from $12 + \log(\text{O}/\text{H}) = 7.3$ (Gr8, Leo A) to $12 + \log(\text{O}/\text{H}) = 9.0$ (M 31¹). These can be compared to the less metallic H II region known, 1Zw18-NW, with a metallicity of $12 + \log(\text{O}/\text{H}) = 7.07$ (Izotov & Thuan 1999), and to the most metal rich H II regions in spiral galaxies, with $12 + \log(\text{O}/\text{H}) \sim 8.9$ (Pilyugin et al. 2007).

2.2 The S2N2 diagram

The sample H II regions were plotted into the original Sabbadin et al. (1977) diagram (Fig. 1) binned into three groups, according to the metallicity adopted for their host galaxies: $7.30 \leq 12 + \log(\text{O}/\text{H}) \leq 8.06$, $8.06 < 12 + \log(\text{O}/\text{H}) \leq 8.40$, and $12 + \log(\text{O}/\text{H}) > 8.40$. The error bars (given in Table A1) are not plotted since they are smaller than, or about the same size as, the symbols. Fig. 1 shows that i) the extragalactic H II regions are not located in the same region as the galactic ones (in contrast to extragalactic PNe, which roughly overlap with the galactic ones,

Table 1. The properties of the galaxies used in this study

Galaxy	M_V	$12 + \log(\text{O}/\text{H})$	Distance [kpc]
M31	-21.2	9.00	760
M33	-18.9	8.40	840
LMC	-18.5	8.37	50
IC 10	-16.3	8.20	660
NGC 6822	-15.96	8.14	500
NGC 3109	-15.80	8.06	1400
SMC	-17.07	8.02	59
IC 1613	-15.3	7.86	725
WLM	-14.4	7.74	925
Sextans B	-14.3	7.56	1320
Sextans A	-14.2	7.49	1450
Leo A	-11.54	7.30	690
Gr8	-12.5	7.30	220

Magrini et al. 2003), and ii) there is a clear correlation between the locations of the H II regions in the diagram and their metallicity, so that as the metallicity increases, both the S2 and N2 line ratios decrease.

3 PHOTO-IONISATION MODELLING

H II regions were modelled using the photo-ionisation code CLOUDY C06.02 (Ferland et al. 1998), assuming a spherical cloud ionised by a single central source of Kurucz (1979, 1991) line-blanketed LTE atmosphere with a temperature

¹ this value given in van den Bergh (2000) may be an overestimation considering the recent studies about the maximum metallicity in spiral galaxies, i.e. Pilyugin et al. (2007). See Sect. 3.

of 45000 K. The electron density was assumed to be 100 cm^{-3} , a typical value for giant extragalactic H II regions (Stasińska 2004). A filling factor of 0.001 was used, based on a study by Muñoz (2001), who determined the filling factor for 73 H II regions in the galaxies NGC 3359 and NGC 7479. For the inner and outer radii of the cloud the default values of CLOUDY were used implying a thin bubble-like cloud surrounding the central object and making the geometry basically plane-parallel. All the chemical elements except the nitrogen were assumed to be of primary origin, i.e. they were scaled according to oxygen. Nitrogen was assumed to be partly primary and partly secondary and it was scaled as $[\text{N}/\text{O}] = 0.08 + [\text{O}/\text{H}]$ (Denicoló et al. 2002) which is in accordance with the observed behaviour of N/O with O/H (Henry et al. 2000). The Orion nebula dust properties were assumed and, as a starting value, Orion nebula abundances were used. With these input parameters a grid of models was calculated for various values of the ionisation parameter and metallicity, and the results are shown in Fig. 2. Further models with higher and smaller densities ($5000 \text{ cm}^{-3}/10 \text{ cm}^{-3}$), different shapes for the ionising sources (blackbody continuum/Kurucz), different filling factor values, up to $= 1$, and cloud sizes and geometry were calculated. In general, the overall changes with respect to the grid of models shown in Fig. 2 were small, with differences $\lesssim 0.15$ dex in the model metallicities.

Fig. 2 shows that, for most of the area occupied by the H II regions, the modelling predicts single valued metallicity and ionisation parameter diagnoses. Only at the highest metallicities and lower ionisation parameter, some folding is present. It is interesting to notice that our modelling gives single valued results down to $\sim \log(\text{H}\alpha/[\text{N II}]) = 0$, while e.g. Melbourne & Salzer (2002) have shown that at $\log(\text{H}\alpha/[\text{N II}]) < 0.45$ the nitrogen line ratio alone ceases to be a good metallicity indicator. The model metallicities agree well with the average values adopted for the different galaxies (Table 1), except for the highest abundances where CLOUDY predicts lower abundance values. In particular, the O/H abundance of M31 is quoted as $12 + \log(\text{O}/\text{H}) = 9.0$ by van den Bergh (2000) but most of the H II regions of M31 occupy a region between 8.4 and 8.8 in Fig. 2. This suggests that the O/H abundance adopted by van den Bergh (2000) for M31 could be significantly overestimated, as it was the case for other spiral galaxies studied by Pilyugin et al. (2007). These authors found a maximum metallicity of $12 + \log(\text{O}/\text{H}) = 8.87$ for the H II regions located at the bulges of the most metal-rich spiral galaxies (see also Bresolin et al. 2004; Pilyugin et al. 2006).

We have compared the O/H abundances estimated through the S2N2 ratio to the abundances calculated by Magrini et al. (2007) for 14 H II regions in M33 (using the empirical ICF method) and by Magrini et al. (2005) for H II regions in Sextans A (8 regions) and Sextans B (7 regions) using CLOUDY modelling. The median differences in $12 + \log(\text{O}/\text{H})$ between the two sets of measurements were 0.24 for Sex A, 0.13 for SexB, and 0.20 for M33, and they do not show any systematics. Considering the quoted errors in the direct O/H abundance determination (≥ 0.1 for Sextans A and B and 0.04-0.25 for M33; Magrini et al. 2005, 2007), these discrepancies seem acceptable.

We have explored the use of the S2N2 indicator for high redshift H II galaxies in the sample of Shapley et al.

(2004). These authors estimated the O/H abundance of several galaxies at $z = 2.1-2.5$; the objects are therefore located at the so called “redshift-desert” ($1.4 < z < 2.5$) where there were virtually no previous determinations of the H II region metallicities. These are crucial objects indeed since that epoch may host the production of a large fraction of the heavy elements present in the local universe. At these redshifts the lines needed for the S2N2 diagram are observable in the near-infrared (*K*-band). We have derived the O/H abundances for the two galaxies in the Shapley et al. (2004) sample for which both the nitrogen and sulphur lines were measured with good accuracy: Q1623-MD 66 ($z = 2.1$) $\text{N}2 = 0.77$; $\text{S}2 = 0.61$, and Q1623-BX 453 ($z = 2.2$) $\text{N}2 = 0.52$; $\text{S}2 = 0.75$ (Shapley et al. (2004), and private communication by Dr. Shapley). We get $12 + \log(\text{O}/\text{H}) = 8.3$ (MD 66) and 8.7 (BX 453), to be compared to the corresponding measurements by Shapley et al. (2004), based on Pettini & Pagel (2004) and Denicoló et al. (2002) N2 calibrations, giving 8.5 and 8.6, respectively, for MD 66, and 8.6 and 8.7, respectively, for BX 453. It is clear that the three sets of measurements differ, albeit the main results of the Shapley et al. (2004) study hold: both galaxies show a high metallicity (in the case of BX 453, comparable to the most metallic nearby spirals) with MD 66 being oxygen poorer than BX 453. In the case of MD 66, our O/H abundance is 0.2-0.3 dex lower than in Shapley et al. (2004). It should be noted that our modelling would permit both the Pettini & Pagel (2004) and Denicoló et al. (2002) O/H values for this galaxy if only the nitrogen line ratio would be considered. The sulphur line ratio helps fixing better the metallicity (see Fig. 2). On the other hand, as mentioned by Shapley et al. (2004), their O/H measurement for BX 453 may be affected by the saturation of $[\text{N II}]/\text{H}\alpha$ - O/H diagnostic at high metallicities. Our modelling shows saturation only at $\text{N}2 \lesssim 0$, and should not thus affect the derived O/H abundances for the galaxies in question here.

One important issue with all O/H measurements in unresolved distant galaxies is, as Shapley et al. (2004) note, that the diffuse interstellar medium in each galaxy (DIG) can make a significant contribution to the observed spectra. According to Moustakas & Kennicutt (2006), the presence of a strong DIG decreases both the N2 and S2 ratios and would thus lead to overestimating the metallicity.

4 THE O/H GRADIENT IN M33

Many galaxies show radial abundance gradients, with the metallicity decreasing from the centre towards the edge of the galaxy. One of the best galaxies to study the abundance gradient is M33, for its closeness, wealth of H II regions, and adequate orientation (almost face-on). Vílchez et al. (1988) derived a global abundance gradient of $-0.12 \text{ dex kpc}^{-1}$ for M33. This measurement was based on their own (direct) abundance measurements in seven H II regions, plus H II region and SNR abundance measurements by other authors (see Vílchez et al. 1988, and references therein). Using H II region data compiled from literature Garnett et al. (1997) derived a similar O/H gradient of $-0.11 \text{ dex kpc}^{-1}$. Monteverde et al. (1997) measured for the stellar (B supergiant) oxygen abundance gradient a value of $-0.16 \pm 0.06 \text{ dex kpc}^{-1}$. However, a more recent estimation of Urbaneja et al.

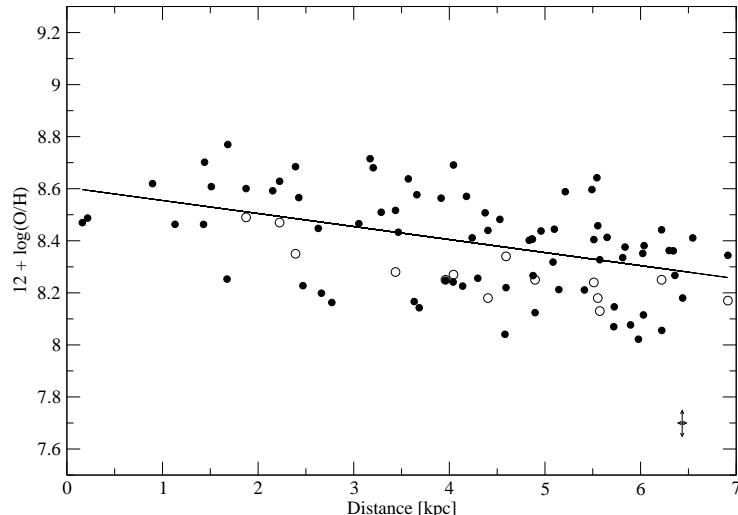


Figure 3. The O/H abundance versus the galacto-centric distance for 76 H II regions of M33. *Filled circles*: abundances derived from our modelling. The solid line is the least square fit to these data. *Open circles*: abundances for 14 H II regions measured by Magrini et al. (2007) using the empirical method.

(2005) for a sample of 11 B-type stars yielded a smaller value of -0.06 ± 0.02 dex kpc^{-1} . Magrini et al. (2004) measured the chemical abundances for 11 planetary nebulae in M33 and found an O/H gradient of -0.14 dex kpc^{-1} , i.e. in agreement with the H II region gradient. Recent abundance measurements of six H II regions by Crockett et al. (2006) show a gradient -0.012 ± 0.011 dex kpc^{-1} , significantly shallower than the previous estimations. However, based on a sample of 5 Beat Cepheids, Beaulieu et al. (2006) inferred again a steeper gradient, -0.16 dex kpc^{-1} . Finally, Pérez-Montero & Díaz (2005) have studied the M33 O/H gradient based on data of ~ 20 H II regions (using both the direct method and the empirical calibrator S_{23}/O_{23}) and early type stars. Albeit they do not provide a numeric value for the gradient, they conclude that the agreement between empirical and direct abundance gradients for M33 is good.

Our data sample includes 76 H II regions in M33, most of which are new measurements by Magrini et al. (2007). O/H abundances for all of them were individually determined with the modelling described above. As for their galacto-centric distances, Magrini et al. (2007) provide coordinates for the centres of the H II regions in their sample, while for the rest of the regions the coordinates are given in Kwitter & Aller (1981). We adopt an inclination angle of 53° , position angle of major axis of 23° and a distance of 840 kpc. The H II regions cover the galacto-centric distances from 0.16 kpc up to 6.91 kpc thus approaching the galactic edge until $0.7R_{25}$ (HyperLeda Extragalactic Database). Fig. 3 shows the resultant oxygen abundances as a function of the galacto-centric distances of the corresponding H II regions. A linear fit gives a value of $12 + \log(\text{O}/\text{H}) = -0.05 (\pm 0.01)$ dex $\text{kpc}^{-1} + 8.60 (\pm 0.05)$.

The errors in the metallicity estimations consist of uncertainties in the modelling plus errors in the measured line

ratios. Due to the large number of parameters involved, realistic errors in the modelling are difficult to estimate. As mentioned in section 2.1, changing the model input parameters to their extreme values can lead into differences of 0.15 dex in the Oxygen abundance. However, for a given model, an error of 0.04 dex in the line ratios (most H II regions in our sample have errors smaller than this) causes an error typically of ~ 0.1 in $12 + \log(\text{O}/\text{H})$. On the other hand, errors in the galacto-centric distances are small, around 0.1 kpc (Magrini et al. 2007). These error-bars are shown in the right-down corner of Fig. 3.

The mean deviation of our data points from the best fit line in Fig. 3 is 0.17 dex. The error bar shown in Fig. 3 plus the possible uncertainty caused by the modelling (0.15 dex, see above) are then enough to explain this scatter. However, there may also exist a real scatter in the abundances. This could be caused by localised gas infall and ineffective mixing or spatially asymmetric chemical enrichment in the galaxy (for theoretical discussion, see Roy & Kunth 1995). These points would certainly be interesting for a detailed future study.

Finally, the oxygen abundance gradient calculated here can be compared to the corresponding gradient by Magrini et al. (2007), based on 14 H II regions with directly measured (ICF) abundances. These measurements are presented in Fig. 3 as open circles. Their gradient is $-0.06 (\pm 0.01)$ dex $\text{kpc}^{-1} + 8.53 (\pm 0.05)$, i.e. in excellent agreement with our determination in this paper. However, our estimation of the metallicity at the centre of M33 is 0.10 higher than the corresponding value by Magrini et al. (2007).

5 CONCLUSIONS

We have shown that the $H\alpha/S[\text{II}]$, $H\alpha/N[\text{II}]$ (S2N2) diagram is a powerful metallicity and ionisation parameter indicator for extragalactic H II regions. A clear advantage of the S2N2 diagram is that the wavelengths of the lines used are close to each other, and thus are not affected by uncertainties in the reddening correction and in the calibration of the instrumental spectral response. The diagram gives unambiguous results over a wide metallicity range. Furthermore, the diagram is especially useful for studies of large samples of new emission line objects of unknown nature, as it separates very efficiently H II regions, PNe, and SNRs from each others, while enabling to estimate their O/H abundances. On the other hand, the $S[\text{II}]$ lines are usually rather weak and may thus not be detectable in all H II regions, whereas the nitrogen lines are possibly influenced by the galaxy's star forming history through the evolution of the N/O abundance ratio.

At low and intermediate metallicities, the diagram is single valued with respect to metallicity; at higher metallicities some folding is present. At the highest metallicities there is also a discrepancy between the O/H abundances predicted by the model and the empirical H II region abundances. However, these can be reconciled if the latter would be significantly lower than previously believed, as proposed by Bresolin et al. (2004) and Pilyugin et al. (2007).

Based on a sample of 76 H II region measurements (12 from the literature and 64 new measurements by Magrini et al. 2007) we have revisited the abundance gradient of M33. We derive for the gradient a value of -0.05 ± 0.01 dex kpc^{-1} in agreement with the recent direct measurements by Magrini et al. (2007).

ACKNOWLEDGEMENTS

The work of K. Viironen was supported by an undergraduate grant from the University of Oulu and a grant from the foundation of Magnus Ehrnrooth, Finland, plus a PhD grant from the Instituto de Astrofísica de Canarias, Spain. Continuous funding from the Spanish Ministerio de Educación y Ciencia (grant AYA-02-00883) is sincerely acknowledged. G. D-I. acknowledges support from Mexican CONACYT projects 42611-F and 50359-F. We are grateful to Dr. Alice Shapley for kindly providing us with the sulphur line data for the galaxies Q1623-MD 66 and Q1623-BX 453.

REFERENCES

- Allain D., Collin-Souffrin S., Joly M., Vigroux L., 1979, *A&A*, 78, 200
- Beaulieu J.-P., Buchler J. R., Marquette J.-B., Hartman J. D., Schwarzenberg-Czerny A., 2006, *ApJ*, 653, L101
- Blair W. P., Kirshner R. P., Chevalier R. A., 1982, *ApJ*, 254, 50
- Bresolin F., Garnett D. R., Kennicutt Jr. R. C., 2004, *ApJ*, 615, 228
- Cantó J., 1981, Herbig-Haro objects - Recent observational and theoretical developments. *ASSL Vol. 91: Investigating the Universe*, p. 95
- Contini T., Treyer M. A., Sullivan M., Ellis R. S., 2002, *MNRAS*, 330, 75
- Crockett N. R., Garnett D. R., Massey P., Jacoby G., 2006, *ApJ*, 637, 741
- Delgado G., Viironen K., Corradi R. L. M., Mampaso A., 2005, in Hidalgo-Gómez A. M., González J. J., Rodríguez Espinosa J. M., Torres-Peimbert S., eds, *Revista Mexicana de Astronomía y Astrofísica Conference Series*, p. 229
- Denicoló G., Terlevich R., Terlevich E., 2002, *MNRAS*, 330, 69
- Dopita M. A., Fischera J., Sutherland R. S., Kewley L. J., Leitherer C., Tuffs R. J., Popescu C. C., van Breugel W., Groves B. A., 2006, *ApJS*, 167, 177
- Dopita M. A., Kewley L. J., Heisler C. A., Sutherland R. S., 2000, *ApJ*, 542, 224
- Dufour R. J., Harlow W. V., 1977, *PASP*, 89, 630
- Dufour R. J., Shields G. A., Talbot Jr. R. J., 1982, *ApJ*, 252, 461
- Ferland G. J., Korista K. T., Verner D. A., Ferguson J. W., Kingdon J. B., Verner E. M., 1998, *PASP*, 110, 761
- Freedman W. L., Wilson C. D., Madore B. F., 1991, *ApJ*, 372, 455
- Galarza V. C., Walterbos R. A. M., Braun R., 1999, *AJ*, 118, 2775
- García-Lario P., Manchado A., Riera A., Mampaso A., Potasch S. R., 1991, *A&A*, 249, 223
- Garnett D. R., Shields G. A., Skillman E. D., Sagan S. P., Dufour R. J., 1997, *ApJ*, 489, 63
- Groves B. A., Heckman T. M., Kauffmann G., 2006, *MNRAS*, 371, 1559
- Henry R. B. C., Edmunds M. G., Köppen J., 2000, *ApJ*, 541, 660
- Hodge P., Miller B. W., 1995, *ApJ*, 451, 176
- Hunter D. A., Hoffman L., 1999, *AJ*, 117, 2789
- Izotov Y. I., Thuan T. X., 1999, *ApJ*, 511, 639
- Kewley L. J., Dopita M. A., 2002, *ApJS*, 142, 35
- Kewley L. J., Dopita M. A., Sutherland R. S., Heisler C. A., Trevena J., 2001, *ApJ*, 556, 121
- Kurucz R. L., 1979, *ApJS*, 40, 1
- Kurucz R. L., 1991, in Philip A. G. D., Uppgren A. R., Janes K. A., eds, *Precision Photometry: Astrophysics of the Galaxy*, p. 27
- Kwitter K. B., Aller L. H., 1981, *MNRAS*, 195, 939
- Lee H., Grebel E. K., Hodge P. W., 2003, *A&A*, 401, 141
- Lee H., Skillman E. D., Venn K. A., 2006, *ApJ*, 642, 813
- Lequeux J., Peimbert M., Rayo J. F., Serrano A., Torres-Peimbert S., 1979, *A&A*, 80, 155
- Lilly S. J., Carollo C. M., Stockton A. N., 2003, *ApJ*, 597, 730
- Magrini L., 2006, in Barlow M. J., Méndez R. H., eds, *IAU Symp. 234*, p. 9
- Magrini L., Leisy P., Corradi R. L. M., Perinotto M., Mampaso A., Vilchez J. M., 2005, *A&A*, 443, 115
- Magrini L., Perinotto M., Corradi R. L. M., Mampaso A., 2003, *A&A*, 400, 511
- Magrini L., Perinotto M., Mampaso A., Corradi R. L. M., 2004, *A&A*, 426, 779
- Magrini L., Vilchez J. M., Mampaso A., Corradi R. L. M., Leisy P., 2007, *A&A* (in press), astro-ph/07053116
- Maier C., Lilly S. J., Carollo C. M., Stockton A., Brodwin M., 2005, *ApJ*, 634, 849
- Melbourne J., Salzer J. J., 2002, *AJ*, 123, 2302
- Moles M., Aparicio A., Masegosa J., 1990, *A&A*, 228, 310

- Monteverde M. I., Herrero A., Lennon D. J., Kudritzki R.-P., 1997, *ApJ*, 474, L107
- Moustakas J., Kennicutt Jr. R. C., 2006, *ApJ*, 651, 155
- Muñoz A., 2001, PhD thesis, Instituto de Astrofísica de Canarias, University of La Laguna
- Nagao T., Maiolino R., Marconi A., 2006, *A&A*, 459, 85
- Pagel B. E. J., Edmunds M. G., Blackwell D. E., Chun M. S., Smith G., 1979, *MNRAS*, 189, 95
- Pagel B. E. J., Edmunds M. G., Smith G., 1980, *MNRAS*, 193, 219
- Peimbert A., Peimbert M., Ruiz M. T., 2005, *ApJ*, 634, 1056
- Peimbert M., Peimbert A., Ruiz M. T., 2000, *ApJ*, 541, 688
- Peimbert M., Torres-Peimbert S., 1974, *ApJ*, 193, 327
- Pérez-Montero E., Díaz A. I., 2005, *MNRAS*, 361, 1063
- Pettini M., Pagel B. E. J., 2004, *MNRAS*, 348, L59
- Pilyugin L. S., Thuan T. X., Vílchez J. M., 2006, *MNRAS*, 367, 1139
- Pilyugin L. S., Thuan T. X., Vílchez J. M., 2007, *MNRAS*, p. 67
- Raimann D., Storchi-Bergmann T., Bica E., Melnick J., Schmitt H., 2000, *MNRAS*, 316, 559
- Richer M. G., Bullesos A., Borissova J., McCall M. L., Lee H., Kurtev R., Georgiev L., Kingsburgh R. L., Ross R., Rosado M., 2001, *A&A*, 370, 34
- Richer M. G., McCall M. L., 1995, *ApJ*, 445, 642
- Riesgo H., López J. A., 2005, *Revista Mexicana de Astronomía y Astrofísica*, 41, 57
- Roy J.-R., Kunth D., 1995, *A&A*, 294, 432
- Sabbadin F., Minello S., Bianchini A., 1977, *A&A*, 60, 147
- Shapley A. E., Erb D. K., Pettini M., Steidel C. C., Adelberger K. L., 2004, *ApJ*, 612, 108
- Skillman E. D., Terlevich R., Melnick J., 1989, *MNRAS*, 240, 563
- Stasińska G., 2004, in Esteban C., García López R., Herrero A., Sánchez F., eds, *Cosmochemistry. The melting pot of the elements*, p. 115
- Stasińska G., 2006, *A&A*, 454, L127
- Tsamis Y. G., Barlow M. J., Liu X.-W., Danziger I. J., Storey P. J., 2003, *MNRAS*, 338, 687
- Urbaneja M. A., Herrero A., Kudritzki R.-P., Najarro F., Smartt S. J., Puls J., Lennon D. J., Corral L. J., 2005, *ApJ*, 635, 311
- van den Bergh S., 2000, *The Galaxies of the Local Group*. Cambridge University Press, Cambridge Astrophysics Series, 35
- van Zee L., 2000, *ApJ*, 543, L31
- van Zee L., Skillman E. D., Haynes M. P., 2006, *ApJ*, 637, 269
- Vermeij R., Damour F., van der Hulst J. M., Baluteau J. P., 2002, *A&A*, 390, 649
- Vílchez J. M., Pagel B. E. J., Diaz A. I., Terlevich E., Edmunds M. G., 1988, *MNRAS*, 235, 633

Table A1. The H II region sample in Local Group galaxies. The errors in the line ratios are given in brackets.

region	$\log(\text{H}\alpha/[\text{N II}])$	$\log(\text{H}\alpha/[\text{S II}])$	reference	region	$\log(\text{H}\alpha/[\text{N II}])$	$\log(\text{H}\alpha/[\text{S II}])$	reference
M31							
K59	0.74 (0.05)	0.66 (0.04)	1	K68	0.39 (0.03)	0.85 (0.03)	1
K70	0.51 (0.03)	0.49 (0.03)	1	K76	0.61 (0.05)	0.49 (0.03)	1
K78	0.57 (0.05)	0.52 (0.03)	1	K81	0.59 (0.05)	0.46 (0.02)	1
K87	0.47 (0.05)	0.46 (0.04)	1	K91	0.47 (0.03)	0.57 (0.03)	1
K92	0.46 (0.03)	0.47 (0.03)	1	K132	0.45 (0.02)	0.68 (0.02)	1
K145	0.42 (0.06)	0.46 (0.05)	1	K244	0.40 (0.03)	0.57 (0.03)	1
K250	0.45 (0.06)	0.66 (0.06)	1	K310	0.55 (0.05)	0.51 (0.04)	1
K314	0.42 (0.03)	0.42 (0.02)	1	K315	0.38 (0.06)	0.60 (0.07)	1
K330	0.46 (0.03)	0.548 (0.015)	1	K343	0.39 (0.03)	0.66 (0.02)	1
K353	0.24 (0.04)	0.28 (0.03)	1	K403	0.89 (0.07)	0.52 (0.03)	1
K414	0.49 (0.03)	0.55 (0.02)	1	K434	0.50 (0.06)	0.40 (0.03)	1
K442	0.61 (0.05)	0.92 (0.04)	1	K446	0.53 (0.04)	0.54 (0.03)	1
K447	0.41 (0.03)	0.62 (0.04)	1	K461	0.18 (0.03)	0.37 (0.03)	1
K480	0.45 (0.06)	0.59 (0.07)	1	K496	0.41 (0.03)	0.54 (0.03)	1
K525	0.43 (0.12)	0.46 (0.06)	1	K526	0.52 (0.03)	0.72 (0.02)	1
K536	0.45 (0.05)	0.42 (0.02)	1	K703	0.49 (0.04)	0.43 (0.02)	1
K722	0.46 (0.05)	0.74 (0.07)	1	K787	0.62 (0.04)	0.46 (0.02)	1
K838	0.53 (0.07)	0.46 (0.05)	1	K851	0.43 (0.12)	0.15 (0.06)	1
K877	0.42 (0.05)	0.57 (0.03)	1	K927	0.45 (0.02)	0.62 (0.02)	1
K931	0.46 (0.05)	0.36 (0.04)	1	K932	0.44 (0.06)	0.52 (0.04)	1
BA75	0.50 (0.04)	0.33 (0.03)	2	BA423	0.50 (0.03)	0.62 (0.02)	2
BA289	0.80 (0.03)	1.05 (0.05)	2				
M33							
CC93	0.54 (0.02)	0.51 (0.02)	3	IC142	0.69 (0.03)	0.77 (0.02)	3
NGC595	0.816 (0.012)	1.06 (0.012)	3	MA2	1.03 (0.03)	1.06 (0.04)	3
NGC604	0.902 (0.003)	0.887 (0.002)	3	NGC588	1.55 (0.03)	1.25 (0.04)	3
MA11	0.82 (0.04)	0.90 (0.04)	4	MA3	1.22 (0.04)	1.33 (0.04)	4
IC131	1.23 (0.04)	1.21 (0.04)	4	MA9a	0.92 (0.04)	0.84 (0.04)	4
IC133	1.39 (0.04)	1.41 (0.04)	4	IC132	1.6 (0.04)	1.39 (0.04)	4
BCLMP 275	0.94 (0.03)	0.75 (0.02)	5	BCLMP 272	0.87 (0.03)	0.44 (0.02)	5
BCLMP 273	0.89 (0.07)	0.54 (0.04)	5	BCLMP 266	0.97 (0.03)	0.69 (0.02)	5
BCLMP 263	0.83 (0.03)	0.507 (0.015)	5	LGC-HII-2	0.77 (0.02)	0.715 (0.013)	5
BCLMP 238	0.98 (0.03)	0.91 (0.04)	5	LGC-HII-3	0.945 (0.011)	0.851 (0.010)	5
BCLMP 240	0.95 (0.03)	0.73 (0.03)	5	BCLMP 289	0.93 (0.04)	0.63 (0.03)	5
BCLMP 218	0.934 (0.009)	0.731 (0.006)	5	BCLMP 258	1.09 (0.02)	0.73 (0.02)	5
BCLMP 288	1.02 (0.02)	1.03 (0.02)	5	MCM2000 Em 24	0.917 (0.012)	0.863 (0.015)	5
BCLMP 220	1.21 (0.02)	0.916 (0.012)	5	CPSDP 194	1.132 (0.005)	1.230 (0.006)	5
BCLMP 256	1.08 (0.03)	1.04 (0.02)	5	VGHC 2-22	1.031 (0.015)	0.969 (0.013)	5
BCLMP 618	0.891 (0.008)	0.825 (0.010)	5	CPSDP 103	0.89 (0.03)	0.66 (0.02)	5
BCLMP 638N	1.36 (0.02)	1.18 (0.02)	5	BCLMP 626	1.02 (0.02)	0.866 (0.014)	5
CPSDP 107	1.21 (0.04)	0.94 (0.03)	5	LGC-HII-4	0.83 (0.02)	0.89 (0.03)	5
BCLMP 45	1.112 (0.007)	1.135 (0.007)	5	BCLMP 207	0.52 (0.02)	0.117 (0.013)	5
BCLMP 640	1.18 (0.06)	0.83 (0.03)	5	BCLMP 55	0.94 (0.03)	0.74 (0.02)	5
CDL2004 52	0.617 (0.006)	0.582 (0.008)	5	CPSDP 221	0.786 (0.009)	0.885 (0.015)	5
LGC-HII-6	0.859 (0.007)	0.99 (0.02)	5	BCLMP 637	1.17 (0.02)	0.93 (0.02)	5
BCLMP 93	0.633 (0.006)	0.617 (0.008)	5	IC 142	0.717 (0.014)	0.68 (0.02)	5
BCLMP 759	0.93 (0.03)	0.74 (0.02)	5	BCLMP 4	0.829 (0.006)	0.985 (0.010)	5
GDK99 128	0.836 (0.003)	0.922 (0.005)	5	CPSDP 316	0.91 (0.03)	0.82 (0.03)	5
BCLMP 670	0.687 (0.012)	0.693 (0.014)	5	LGC-HII-7	1.09 (0.03)	0.96 (0.07)	5
VGHC-2-84	0.912 (0.005)	1.040 (0.009)	5	BCLMP 709	0.832 (0.010)	0.867 (0.014)	5
CPSDP 323	0.84 (0.02)	0.76 (0.03)	5	CPSDP 325	0.67 (0.05)	0.46 (0.06)	5
BCLMP 721	0.93 (0.03)	0.69 (0.02)	5	BCLMP 682	0.75 (0.03)	0.70 (0.02)	5
BCLMP 715	0.78 (0.02)	0.50 (0.02)	5	CPSDP 189	0.80 (0.06)	0.59 (0.05)	5
BCLMP 659	0.95 (0.03)	0.91 (0.03)	5	LGC-HII-8	0.89 (0.04)	0.62 (0.02)	5
BCLMP 680	0.70 (0.02)	0.64 (0.02)	5	BCLMP 717	0.950 (0.010)	0.880 (0.010)	5
LGC-HII-10	0.87 (0.03)	0.78 (0.02)	5	BCLMP 749	0.927 (0.012)	0.96 (0.02)	5
BCLMP 649	1.04 (0.03)	0.90 (0.03)	5	BCLMP 705	0.75 (0.03)	0.81 (0.06)	5
LGC-HII-11	1.16 (0.02)	1.00 (0.02)	5	MCM2000 Em 59	0.71 (0.02)	0.63 (0.02)	5
BCLMP 757	0.99 (0.02)	0.896 (0.012)	5	BCLMP 657	1.02 (0.04)	0.86 (0.04)	5
LGC-HII-12	0.91 (0.02)	0.77 (0.02)	5	BCLMP 754	1.01 (0.02)	0.67 (0.02)	5
LGC-HII-13	1.24 (0.05)	1.11 (0.06)	5	BCLMP 756	0.995 (0.014)	0.88 (0.02)	5

Table A1 – continued

region	$\log(\text{H}\alpha/[\text{N II}])$	$\log(\text{H}\alpha/[\text{S II}])$	reference	region	$\log(\text{H}\alpha/[\text{N II}])$	$\log(\text{H}\alpha/[\text{S II}])$	reference
LMC							
N160A1	1.18 (0.04)	1.10 (0.04)	6	N160A2	1.19 (0.05)	1.13 (0.05)	6
N159-5	1.13 (0.04)	0.95 (0.03)	6	N157B	1.11 (0.05)	0.73 (0.03)	6
N11A	1.23 (0.04)	1.14 (0.05)	6	N83B	1.10 (0.03)	1.04 (0.03)	6
N79A	1.08 (0.03)	1.02 (0.03)	6	N4A	1.33 (0.03)	1.25 (0.03)	6
30Dor1	1.74 (0.04)	1.62 (0.03)	7	30Dor2	1.78 (0.04)	1.49 (0.03)	7
30Dor3	1.56 (0.03)	1.53 (0.03)	7	30Dor4	1.35 (0.03)	1.26 (0.03)	7
NGC2079	1.29 (0.12)	1.12 (0.11)	7	IC2111	1.11 (0.07)	1.06 (0.09)	7
N157	1.53062	1.43861	8	N159	1.28913	1.12494	8
N8	1.39 (0.03)	1.20 (0.03)	9	N11B	1.28	1.11	10
IC 10							
HL106a	0.92 (0.06)	0.62 (0.03)	11	HL106b	1.16 (0.06)	1.03 (0.06)	11
HL111b	0.96 (0.03)	0.72 (0.02)	11	HL111c(WR)	1.31 (0.09)	1.12 (0.02)	11
HL111e	1.09 (0.04)	0.81 (0.02)	11	HL30	1.07 (0.08)	0.84 (0.06)	11
HL45	1.48 (0.05)	1.172 (0.011)	11	HL111d+e	1.25 (0.07)	1.11 (0.08)	11
HL77	1.2 (0.1)	1.03 (0.09)	11	IC10(1)	1.42 (0.03)	1.21 (0.03)	12
IC10(2)	1.39 (0.03)	1.26 (0.03)	12				
NGC6822							
Ho11	1.27 (0.15)	1.03 (0.15)	13	HuX	1.74 (0.10)	1.30 (0.07)	13
HuV	1.71 (0.07)	1.38 (0.03)	13	Ho14	0.86 (0.10)	0.80 (0.11)	13
Ho13	1.28 (0.08)	0.76 (0.06)	13	Ho15	1.50 (0.15)	1.20 (0.08)	13
HuV	1.75 (0.02)	1.386 (0.013)	14	HuX	1.60 (0.03)	1.21 (0.02)	14
HK16	0.91 (0.13)	0.45 (0.06)	15	Ho12	1.03 (0.09)	0.27 (0.03)	15
HuV	2.31 (0.04)	1.45 (0.03)	15	Kalfa	2.09 (0.06)	1.49 (0.02)	15
KD28e	1.61 (0.07)	1.11 (0.08)	15				
SMC							
N88A	1.73 (0.03)	1.47 (0.03)	6	N66	1.67 (0.05)	1.22 (0.04)	6
N12A	1.48 (0.06)	1.08 (0.06)	9	N12B	1.66 (0.06)	1.06 (0.06)	9
N22	1.57 (0.06)	1.23 (0.06)	9	N25	1.37 (0.06)	1.02 (0.06)	9
N76SW	1.49 (0.06)	0.94 (0.06)	9	N83	1.47 (0.06)	1.17 (0.06)	9
N90	1.53 (0.06)	1.24 (0.06)	9	NGC346	1.873 (0.005)	1.365 (0.003)	16
N81	1.66 (0.12)	1.4 (0.1)	17				
WLM							
WLM1	1.43 (0.09)	0.85 (0.04)	18				
SextansA							
HSK2	1.60 (0.12)	0.94 (0.04)	19	HSK3	1.57 (0.14)	1.06 (0.06)	19
HSK7	1.54 (0.10)	1.05 (0.04)	19	HSK9	1.41 (0.08)	0.94 (0.04)	19
HSK16	1.59 (0.11)	0.89 (0.03)	19	HSK19	1.47 (0.13)	0.85 (0.03)	19
HSK23	1.40 (0.07)	0.96 (0.03)	19	HSK24	1.45 (0.13)	0.79 (0.04)	19
SextansB							
SextB1	1.38 (0.09)	0.91 (0.03)	17	SextB3	1.44 (0.14)	0.85 (0.04)	17
SHK2	1.318 (0.014)	0.804 (0.013)	19	SHK3	1.15 (0.07)	0.54 (0.02)	19
SHK5	1.60 (0.05)	0.95 (0.03)	19	SHK6	1.10 (0.11)	0.44 (0.04)	19
SHK7	1.13 (0.04)	0.77 (0.03)	19	SHK10	1.20 (0.02)	0.812 (0.011)	19
HIH	1.50 (0.04)	0.92 (0.02)	19	SextB	1.62 (0.12)	0.84 (0.11)	20
LeoA							
-101-052	1.89 (0.10)	1.18 (0.04)	21	-091-048	1.58 (0.08)	1.10 (0.05)	21
+069-018	1.52 (0.07)	0.98 (0.05)	21	+112-020	1.62 (0.04)	1.02 (0.03)	21
Gr8							
-019-019	1.52 (0.03)	1.01 (0.03)	21	-013-032	1.30 (0.05)	0.76 (0.04)	21
-012-022	1.53 (0.03)	0.97 (0.03)	21	-002-012	1.34 (0.03)	0.74 (0.03)	21
+001-008	1.52 (0.04)	0.82 (0.03)	21	+001+027	1.55 (0.05)	1.01 (0.04)	21
+004-006	1.37 (0.03)	0.81 (0.02)	21	+008-011	1.46 (0.03)	0.99 (0.02)	21

Table A1 – *continued*

region	$\log(\text{H}\alpha/[\text{N II}])$	$\log(\text{H}\alpha/[\text{S II}])$	reference	region	$\log(\text{H}\alpha/[\text{N II}])$	$\log(\text{H}\alpha/[\text{S II}])$	reference
IC 1613							
IC1613.13	1.32 (0.11)	0.87 (0.07)	22				
NGC 3109							
NGC3109.6.6	1.24 (0.12)	0.92 (0.08)	22				

References: (1) Galarza et al. (1999)^a, (2) Blair et al. (1982), (3) Vílchez et al. (1988), (4) Kwitter & Aller (1981), (5) Magrini et al. (2007), (6) Vermeij et al. (2002), (7) Peimbert & Torres-Peimbert (1974), (8) Dufour et al. (1982), (9) Dufour & Harlow (1977), (10) Tsamis et al. (2003), (11) Richer et al. (2001), (12) Lequeux et al. (1979), (13) Pagel et al. (1980), (14) Peimbert et al. (2005), (15) Lee et al. (2006), (16) Peimbert et al. (2000), (17) Hunter & Hoffman (1999), (18) Skillman et al. (1989), (19) Magrini et al. (2005), (20) Moles et al. (1990), (21) van Zee et al. (2006), (22) Lee et al. (2003)

^a Galarza et al. (1999) present line measurements with various apertures, covering different parts of the H II region or the whole complex in their sample. We have used the fluxes corresponding to the whole complex, when available, or to the brightest zone in each region.